Theoretical and experimental investigation of electronic structure and relaxation of colloidal nanocrystalline indium phosphide quantum dots

Randy J. Ellingson,[1] Jeff L. Blackburn,[1] Jovan Nedeljkovic,[1] Garry Rumbles,[1] Marcus Jones,[1] Huaxiang Fu,[2] and Arthur J. Nozik[1]

[1]*Center for Basic Science, National Renewable Energy Laboratory, Golden, Colorado 80401*

[2]*Department of Physics, Rutgers University, Camden, New Jersey 08102*

(Received 23 September 2002; published 7 February 2003)

We present results of theoretical studies of the electronic structure, and experimental studies of electronic relaxation dynamics, for colloidally synthesized InP quantum dots (QD's). Detailed theoretical calculations of the electronic structure of a 41.8 Å diameter InP QD, based on an atomistic pseudopotiential approach, are presented and discussed in the context of experimental measurements. Using femtosecond transient absorption (TA) spectroscopy, we find that the rate of relaxation of photogenerated excitons to the lowest-energy exciton level varies depending upon excitation energy and surface chemistry. Etching the QD's passivates surface electron traps and yields enhanced carrier cooling, which we ascribe to improved confinement of charge carriers to the QD core. When exciting near or slightly above the first exciton state, we observe a subpicosecond decay of the band edge TA bleach signal which we attribute to a thermalization process. We also present size-selective transient absorption measurements providing experimental evidence which confirms the existence of two *s*-like exciton states spaced by ~100 meV.

DOI: 10.1103/PhysRevB.67.075308 PACS number(s): 73.22.−f, 71.35.−y, 73.21.−b

INTRODUCTION

Nanomaterials exhibit unique physical and chemical properties, including size-dependent electronic structure arising from confinement of the charge carriers within particles smaller than the bulk material's Bohr exciton diameter. Colloidally prepared semiconductor quantum dots (QD's) lie typically in the 10 to 100 Å diameter range. Quantum dots display clear quantum size effects, including emission blueshifted from that of the bulk, and absorption spectra which include discrete exciton transition features. Colloidal QD's expose a large fraction of their atoms to the surface, with ~50% of atoms in contact with the surface for a 20 Å diameter InP QD; as such, the surface-specific electronic structure can play a significant role in certain scattering and relaxation processes. Colloidal III-V and II-VI QD's are typically prepared in the presence of organic surfactants, which stabilize the particle surface against oxidation, partially passivate surface states, and serve to solubilize the particles in nonpolar organic solvents. Trioctylphosphine (TOP) and trioctylphosphine oxide (TOPO) are used frequently to cap III-V and II-VI semiconductor QD's, and provide large potential barriers to both the electron and the hole. Semiconductor QD's provide a material system well suited to studying interactions between charge carriers, which may be strongly confined to the dot core as an exciton or separated via surface trap states or scavenger molecules. The recent demonstration of room temperature lasing using colloidal CdSe QD's demonstrates their potential for application to optically pumped devices.[1]

Colloidal semiconductor QD's show a sparsity of electronic energy levels due to quantum confinement. An InP nanocrystal of 35 Å diameter has an energy spacing between the first and second lowest exciton states of ~53 meV,[2] more than the longitudinal optical (LO) phonon energy (43 meV).[3] The spacing between the second and third Γ-like exciton states is 47 meV, again, more than the LO phonon energy. The large interstate energy spacing and the concomitant potential for slowed cooling of excitons is known as the "phonon bottleneck."[4–6] Conduction band electrons have traditionally been identified as the charge carriers subject to slowed cooling, because the smaller electron effective mass yields single-particle conduction levels spaced further apart than those of the hole in the valence band. However, recent results on CdSe QD's have shown that interaction between the electron and hole facilitates electronic relaxation.[7,8] The effect for colloidal CdSe QD's has been described as an Auger-like process in which the hot electron can scatter its excess energy to the hole, which can then cool efficiently via phonon scattering, relaxing quickly via the denser manifold of valence band states. In spite of the Auger-like cooling mechanism, slowed relaxation has been observed for hot electrons[7,8] as well as for hot holes.[9] Slowed relaxation of hot carriers, which may enable more efficient photoenergy conversion, requires that the dynamics of charge separation of the electron and hole compete with electronic relaxation. To study the electronic structure and electronic relaxation in InP QD's, we have conducted transient absorption (TA) experiments on InP QD's using an interband pump followed by a white light probe over the range of approximately 440 to 760 nm. Our spectral TA measurements yield excellent agreement with theoretical excitonic structure calculations. Dynamical measurements on InP QD's indicate some dependence of electronic relaxation on the nature of the nanocrystal surface. In particular, we observe slightly faster relaxation for etched QD's than is observed for unetched QD's. Previous measurements on InP QD's suggested evidence of surface hole trapping dynamics competing with electronic relaxation.[10] The time-dependent TA data presented here, while niether corroborating nor contradicting the role of surface hole traps, does provide further evidence that improving

confinement of the charge carriers to the dot core increases the electronic relaxation rate.

THEORETICAL

Electronic structure calculations on colloidal semiconductor QD's provide information important for predictive and interpretive uses. To explain the physical origins of observed excitonic peaks, we calculated excitonic energies using the atomistic pseudopotential method (APM). Specifically, the computation is done in two steps.

First, the single-particle orbital energies and wave functions are computed by solving the Schrödinger equation

$$\left\{ -\frac{1}{2}\nabla^2 + \sum_{R_n} \sum_{\tau_\alpha} v_\alpha(\mathbf{r}-\mathbf{R}_n-\tau_\alpha) \right\} \psi_i = \varepsilon_i \psi_i , \qquad (1)$$

where $v_\alpha(\mathbf{r}-\mathbf{R}_n-\tau_\alpha)$ is the screened, nonlocal pseudopotential[11] for the atom of type α located at site τ_α in cell $\mathbf{R}_n$ and ε_i is the single particle orbital energy. The APM approach, counting the existence of each atom in colloidal dots, allows us to study near-band edge electronic structure of InP QD's and also the effects of surface states due to In or P dangling bonds.[12] This approach is accurate and reliable: the theoretical lowest-energy excitonic gap[12] of fully passivated InP dots agree well with the experimental measurements,[13] and moreover, the predicted surface states were confirmed by experimental observations.[14] Here we present calculation results of the electronic structure of a 41.8 Å diameter InP QD. To study the origin of each peak in the experimental spectrum over a wide energy range, a large number of single-particle states, including 32 valence states and 16 conduction states, are calculated. The calculated orbital energy and its envelope-function character (*s*,*p*,*d*, or *f*) of each state are given in Table I. With spin-orbit coupling included, the first two highest-energy valence states are doubly degenerate *s*-like states, and the next two highest-energy valence states are *p*-like. The energy separation of *s*-like and *p*-like valence states is ~38 meV, which is comparable to the LO phonon energy in InP dots. The fifth valence state in Table I is the spin-orbit split-off *p*-like state, while the sixth valence state is the split-off *s*-like state. Our calculation thus shows that the spin-orbit splitting is smaller for the *p*-like than for the *s*-like valence states in the 41.8 Å dot. For conduction states, the lowest-energy level is predominantly *s*-like. Unlike small InP dots for which the second lowest-energy conduction level is *L*-like, the second lowest level for a 41.8 Å dot is Γ-like with *p* envelope function. The envelope characters given in Table I assist with understanding which single-particle states contribute to the interband exciton transitions. In Table I, it can also be seen that, for those states far from the band edge (e.g., the 25th valence state), there is a strong mixing of envelope parity (i.e., *p*, *f* of odd-parity mixing with *d* of even parity), and it is generally not possible to assign a well-defined principal quantum number to each dot state as in atomic physics.

As a second step, we calculated the excitonic energy levels and wave functions using the configuration interaction (CI) approach.[2] Since the exchange splitting is much smaller than the Coulomb interaction and the relevant energy resolution of current experiment does not contain the exciton fine structure due to exchange interaction, we include only the dominant Coulomb interaction in our CI calculation. For each exciton state, the transition energy consists of the spacing between the contributing single particle electron and valence states minus the exciton binding energy. The theoretical transition spectrum obtained from our CI calculation is illustrated in Fig. 1, revealing seven major peaks. We identify the single-particle states that are responsible for these major peaks, and the results are given in Table II. The peak at 1.84 eV arises from the transition between the two highest-energy *s*-like valence states and the lowest *s*-like conduction state. The peak at 1.94 eV comes from the transition between the split-off *s*-like valence state and the lowest conduction state. The two peaks at 2.18 and 2.24 eV are attributed to the transitions from *p*-like valence states to *p*-like conduction states. The theoretical peaks from 2.3 to 2.7 eV are mainly due to the *d*-like single-particle states. Comparing the experimental spectrum with that predicted by theory shows that each of the broad experimental peaks at ~1.9 or ~2.15 eV actually result from two different transitions. Similarly, the broad experimental peak at ~2.5 eV results from three exciton transitions.

EXPERIMENTAL

Indium phosphide QD's were synthesized using standard colloidal methods, in the presence of trioctylphosphine oxide (TOPO) and trioctylphosphine (TOP), as previously reported.[15] The zinc blende InP nanocrystals studied here have a mean diameter of 42 Å, as determined by the energy of their first exciton absorption,[16] with a size distribution of ~±6%. The organic capping molecules TOPO and TOP serve to solubilize the dots for suspension in organic solvents such as hexane and toluene, and also effect partial passivation of surface dangling bonds.

All absorption, emission, and TA measurements have been conducted at room temperature on colloidal QD solutions contained in fused silica cuvettes of 1 or 2 mm path length. In order to investigate the spectroscopic properties for different surface chemistries, we have made measurements on InP QD samples in hexane, both (1) as-prepared and (2) etched. As prepared, the QD's are capped with TOP/TOPO; this sample exhibits weak (~1% quantum yield at room temperature) band edge photoluminescence (PL) and significant emission at lower energies which we attribute to deep trap emission. We prepare the etched sample using a dilute methanolic solution of HF or NH_4F in the presence of TOPO/TOP.[15] Etched dots show a factor of ten or more increase in the near-band-edge PL, and a reduction in the relative intensity of near infrared emission indicative of improved passivation of deep surface trap states. Steady state absorption measurements were made on a Cary 500 double spectrophotometer at 1 nm spectral resolution. Steady-state emission spectra were recorded for 400 nm excitation using a Fluorolog-3 spectrometer with CCD detection system. Excitation light generated by a 450 W xenon arc lamp was selected for 1 nm bandwidth using a double monochrometer.

TABLE I. Valence (a) and conduction (b) single-particle states for a 41.8 Å diameter InP quantum dot. Columns 3–6 indicate the percentage distribution of envelope angular momentum components for each single-particle level. Energies are relative to vacuum.

State index	Energy (eV)	*s*	*p*	*d*	*f*
	(a) Valence states				
1	−6.0303	76.9	9.5	8.0	1.7
2	−6.0303	76.9	9.5	8.0	1.7
3	−6.0679	2.7	84.9	5.7	2.6
4	−6.0679	2.7	84.9	5.7	2.6
5	−6.1268	0.2	84.2	6.0	4.5
6	−6.1275	69.8	4.8	17.7	2.1
7	−6.1386	2.0	60.5	11.5	16.1
8	−6.1386	2.0	60.5	11.5	16.1
9	−6.1403	0.4	5.3	77.5	5.7
10	−6.1403	0.4	5.3	77.5	5.7
11	−6.1542	0.0	2.9	80.9	4.5
12	−6.1834	40.2	4.2	37.4	3.6
13	−6.1835	40.2	4.1	37.3	3.7
14	−6.1961	0.5	2.2	0.7	82.5
15	−6.2261	37.3	2.1	33.4	5.8
16	−6.2473	0.9	25.4	11	36.9
17	−6.2496	3.0	21.8	14.8	35.2
18	−6.2544	5.1	21.3	7.2	47.3
19	−6.2549	3.5	23.1	16.5	36.4
20	−6.2552	1.9	25.9	18.8	27.5
21	−6.2641	2.0	35.8	21.1	21.1
22	−6.2657	1.5	33.1	14.6	30.5
23	−6.2665	5.3	38.3	8.6	29.1
24	−6.2880	1.6	32.7	15.2	19.3
25	−6.2852	1.9	26.1	20.4	20.9
26	−6.3054	1.7	14.5	17.9	12.1
27	−6.3114	2.4	14.0	13.8	24.9
28	−6.3119	3.8	12.8	18.5	26.5
29	−6.3245	4.5	17.5	22.2	11.2
30	−6.3316	5.3	21.7	19.0	11.4
31	−6.3544	11.8	9.0	26.8	9.0
32	−6.3641	8.4	8.1	27.7	9.5
	(b) Conduction states				
1	−4.0608	82.5	10.6	1.5	1.4
2	−3.7855	5.7	73.2	10.5	2.6
3	−3.7855	5.7	73.2	10.5	2.6
4	−3.7771	5.3	73.1	10.5	2.9
5	−3.7019	0.8	1.2	6.3	0.8
6	−3.7017	0.7	1.1	6.4	0.8
7	−3.7017	0.7	1.1	6.4	0.8
8	−3.6994	2.7	0.3	3.7	0.8
9	−3.6324	1.3	3.3	1.3	16.5
10	−3.6312	0.1	6.1	1.0	9.6
11	−3.6298	0.1	6.3	0.9	9.3
12	−3.6298	0.1	6.3	0.9	9.3
13	−3.5879	4.6	0.9	5.6	5.0
14	−3.5599	1.9	9.0	58.5	12
15	−3.5568	1.8	5.7	39.1	7.5
16	−3.5540	1.6	2.6	22.3	3.9

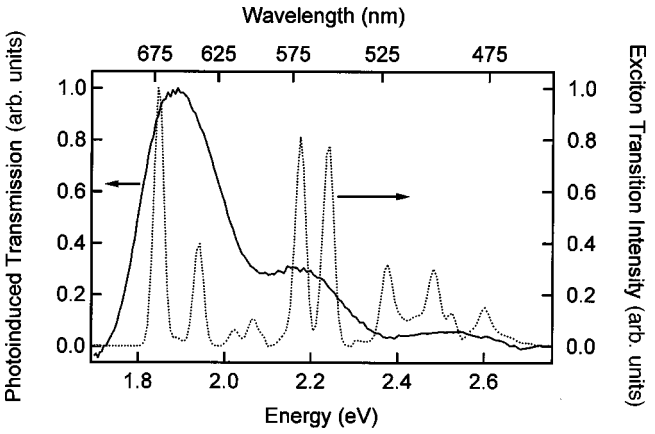

FIG. 1. Theoretical excitonic spectrum (dashed line) for a sample of 41.8 Å diameter InP quantum dots. The transition intensity is proportional to the absorption coefficient, and consists of a sum of the oscillator strengths for various excitonic transitions. The solid line shows the measured photoinduced bleach spectrum, at a delay of 1.0 ps, for a sample with average size of ~42 Å diameter. Theoretical transition peaks correspond to those listed in Table II. The two small peaks between 2.0 and 2.1 eV originate from transitions between valence states 12, 13, and 15, and conduction state 1. We refer to the broad features observed in the experimental spectrum at 1.9, 2.15, and 2.5 eV as the "**S**," "**P**," and "**D**" exciton transitions, respectively.

The front-face emission from the sample was collected at 22.5° relative to the excitation beam and passed through a single monochrometer before being imaged on the CCD array.

Our transient absorption experimental setup, previously described in detail,[17] is based on a Clark-MXR CPA-2001 regeneratively-amplified Ti:sapphire laser, operating at 989 Hz. The 775 nm output pulses pump a TOPAS OPA capable of output in the range of 290 nm to 2.4 μm; in addition, a fraction of the 775 nm pulse train is focused onto a 2 mm sapphire window to generate white light (WL) probe pulses which range from approximately 440 to 950 nm. We use a chirp-corrected approach for our fixed-time spectral TA measurements, in which the arrival times for the various WL wavelength components are determined using two-photon absorption (a fixed visible OPA wavelength mixed with the

TABLE II. Theoretical exciton transition peaks, and those valence and conduction states which contribute to the transitions.

	Exciton transitions	
Peak position (eV)	Valence states	Conduction states
1.84	1, 2	1
1.94	6	1
2.18	3, 4	2, 3, 4
2.24	5	4
2.24	7, 8	2, 3
2.38	17–25	2, 3, 4
2.48	9, 10, 11	14, 15
2.60	17, 19, 21, 22, 24, 25	14

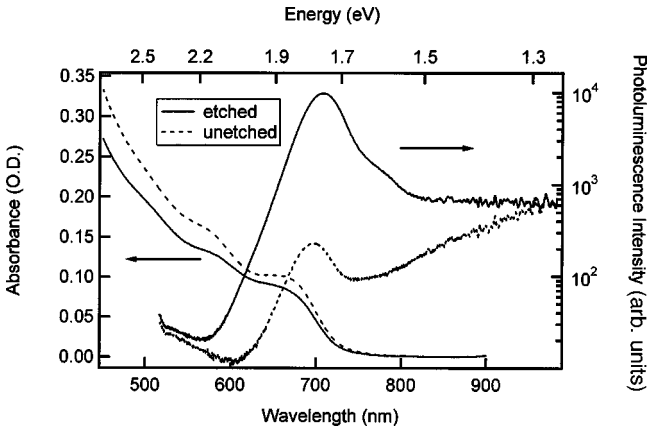

FIG. 2. Absorption and emission from as-prepared (unetched) and etched 42 Å diameter InP QD's in hexane. Note the logarithmic scale for emission intensity.

WL) in a 0.5 mm thick ZnO crystal.[18]

The visible pump and WL probe pulses are focused to spot sizes of ~500 and 125 μm, respectively. Spatially filtering the visible pump beam is used to improve the transverse mode quality.[17] We utilize standard TA measurement techniques in which a visible pump pulse photoexcites the dots at or above the first exciton transition, and the WL pulse probes the induced change in absorption at a specific energy, e.g., the energy corresponding to the first exciton absorption. We determine the system response using two-photon absorption between pump and probe pulses in ZnO. Two effects contribute to the pump-induced change in absorption. At short times, the carrier-induced Stark effect results in a derivativelike differential absorption spectrum. As the excitons cool to the band edge on the ~100 fs time scale, state-filling induced bleaching of the absorption dominates the TA signal.

We determine the solution nanoparticle concentration from the decadic extinction coefficient ε as previously described.[17] The average excitation density per particle $\langle N_0 \rangle$, is computed using the product of the pump fluence (j_p, photons per pulse per cm^2) and the absorption cross section σ_a: $\langle N_0 \rangle = j_p \sigma_a$. Measurements are typically made exciting at $\langle N_0 \rangle \leq 0.5$ electron-hole pairs per dot, which simplifies experimental interpretation by largely avoiding multipair Auger recombination effects.[19]

RESULTS AND DISCUSSION

Figure 2 shows absorption and emission data for unetched and etched samples of 42 Å diameter InP QD's in hexane. Absorption features associated with exciton transitions are evident near 660, 570, and 500 nm. Following etching, the exciton features broaden indicating a slightly increased size distribution due to the etching process. For the unetched sample, band edge emission is extremely weak while emission at lower energies associated with deep level traps is relatively strong. In contrast, etching strongly increases band-edge emission while significantly reducing the relative strength of the deep trap emission. Clearly the surface chemistry affects one or more of the relative rates of radiative, nonradiative, and deep trap related recombination.

Samples with sufficiently narrow size distribution reveal TA features corresponding to higher energy exciton transitions. The solid line in Fig. 1 shows the normalized TA spectrum at 1 ps delay following photoexcitation at 3.2 eV to a per-dot average exciton population of $\langle N_0 \rangle = 0.4$. Although the calculated excitonic structure (dotted line in Fig. 1) reveals multiple transitions within each of the broad experimental peaks, we refer here to the experimental exciton features at 1.9, 2.15, and 2.5 eV as the "**S**," "**P**," and "**D**" peaks, respectively. The calculated envelope function character of the single particle levels contributing to the **S**, **P**, and **D** experimental peaks are indeed primarily *s*-, *p*-, and *d*-like, respectively (see Tables I and II). However, the calculated excitonic transitions indicate that broadening produces an experimental spectrum concealing additional structure corresponding to two or three transitions within each of the **S**, **P**, and **D** experimental peaks. Thus, the excitonic ladder along which relaxation occurs for core-confined electron-hole pairs consists of more states than are resolvable spectroscopically. Two important issues to note are the following: first, the excitonic ladder also includes states which are orbitally forbidden. While these states offer only very weak oscillator strength for absorption, they are accessible to cooling excitons and therefore further increase the state density and reduce the magnitude of energy gaps between exciton states. Secondly, our calculations do not include the effects of electron-hole exchange and the crystal field, both of which split the exciton states and result in fine structure which significantly increases the number and density of exciton states.

There are two distinct ways to discuss electronic relaxation in QD's: one can speak of the cooling of electrons and holes separately through conduction and valence band levels, or one can speak of exciton cooling. For strongly confining QD's in which the electron and hole wave functions are confined to the dot core as an exciton, the electron and hole are correlated and quantum mechanically occupy *excitonic* states rather than single particle levels. On the other hand, if one charge carrier wave function transfers from the dot core states to a surface state or external state (i.e., by charge separation to a surface trap or surface scavenger molecule),[7,8] the remaining core-confined carrier can be said to occupy single particle levels, with a substantial reduction in the Coulomb interaction. For real-world dots, even charge-separated carriers will be imperfectly screened from one another, and the spectrum of interaction thus ranges from the strongly correlated "pure exciton" to weakly interacting. Consider the case where two types of dots exist within a colloidal QD sample, consisting of (1) dots for which the electron and hole are confined to the particle core as an exciton and (2) dots for which one carrier remains confined while the other traps at the surface. If the extension of the wave function to surface trap states is sufficiently fast to compete with electronic relaxation, two different relaxation scenarios may occur depending upon the trapping time: relaxation of the core-confined exciton, or electronic relaxation with a reduced Coulomb interaction. The distinction is important in part because while for 42 Å diameter InP QD's the spacing between the two lowest conduction levels suggests an intraband gap of 275 meV, the gap between the two lowest exciton transi-

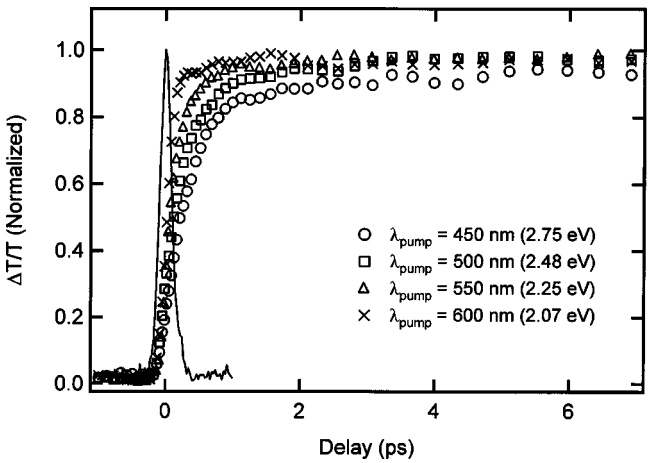

FIG. 3. Dynamics for the unetched 42 Å diameter InP QD sample showing variation in rise time of **S** exciton bleach signal at 660 nm for excitation wavelengths between 450 and 600 nm. Exciton transitions associated with the **P** bleach may be excited only by 550 nm and shorter wavelength excitation. The solid line shows the two-photon absorption cross correlation in ZnO for 2.07 eV excitation.

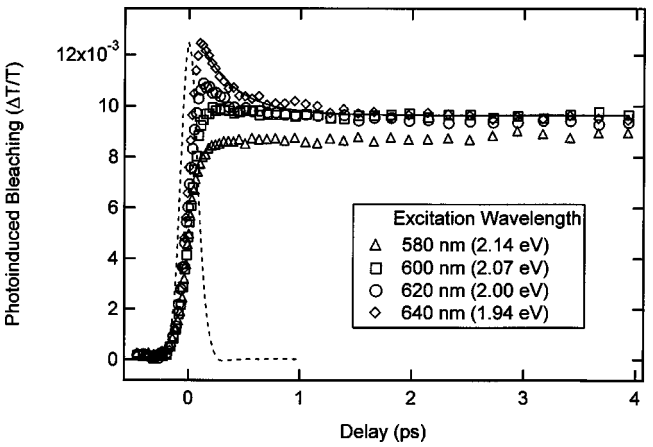

FIG. 4. Transient absorption dynamics probed at 660 nm (1.88 eV, the **S** bleach peak) for unetched 42 Å diameter InP QD's in hexane, as a function of excitation energy, excited to a level of $\langle N \rangle = 0.2$. The solid line shows the exponential fit for 1.94 eV excitation energy, and indicates a relaxation time of 315 ± 25 fs. The dashed line shows the two-photon absorption cross correlation in ZnO for 2.07 eV excitation.

tions is just 44 meV.[17] Relative to the intraband spacing of conduction electron (single particle) levels, the magnitude of the gaps between exciton states, on which the phonon bottleneck may depend, decreases significantly if the electron and hole cool together through the exciton states.

The rise time of the **S** exciton bleach signal at 660 nm (1.88 eV) correlates to the dynamics of electronic relaxation to the *s*-like exciton states at 1.84 and 1.94 eV. Therefore, when photoexciting excitons above the highest *s*-like transitions (1.94 eV), the build-up of the **S** bleach provides a measure of relaxation to exciton states involving the $1S_e$ level. Figure 3 presents dynamics of the **S** bleach for the unetched sample, as a function of excitation wavelength, for a photoexcited average per-dot exciton density of 0.2. As expected, the **S** bleach build-up time increases for increasing excitation photon energy, reflecting the fact that relaxation from higher energy states proceeds more slowly. The rise time of the **S** bleach signal can be well fit using two exponentials, and the increasing rise time with increasing initial exciton energy is reflected in both the faster and slower components. Analysis of the relaxation rate using a model based on the calculated excitonic structure is in general problematic: for example, our sample size distribution blurs the existence of the dual-peaked nature of the **S** bleach peak. However, we believe that the two components arise from the carrier-induced Stark effect (faster) and the effect of state filling from higher exciton states (slower). Experimentally we measure the dynamics at the peak of the **S** exciton bleach at 660 nm (1.88 eV), and we are currently unable to resolve the separate contributions of the 1.84 and 1.94 eV exciton transitions. Excitation at 600 nm (2.07 eV) yields time constants of 60 and 300 fs, indicating very fast relaxation. Excitation at 550 nm (2.25 eV) permits excitation into the highest of the two *p*-like exciton states, and the dynamics of the **S** bleach build up indicate components of 190 fs and 1 ps. Pumping at 500 nm (2.48 eV) yields rise time components of 250 fs and 1.5 ps, while excitation at 450 nm (2.75 eV), which is well above the *p*-like exciton transitions, yields components of 360 fs and 6.5 ps, indicating substantially slowed relaxation.

As previously reported, photoexcitation within about 100 meV of the **S** bleach peak results in the appearance of a $\sim < 1$ ps relaxation component within the **S** bleach dynamics.[17] The short time decay component of the **S** bleach relaxation, shown in Fig. 4 as a function of excitation energy, becomes decreasingly prominent for increasing excitation energy, and vanishes for photoexcitation wavelengths shorter than 600 nm. Although we earlier attributed this initial relaxation to hole cooling,[17] our continued investigation has revealed that the decay component persists even when photoexciting at or below the lowest *s*-like exciton energy. The lowest excitation energies prepare the exciton in a state without significant excess energy above the band edge, and thus hole-related cooling effects are not expected. The short time relaxation is present independent of QD etching, and shows no polarization anisotropy for our room temperature measurements. The fast decay is most prominent when the exciton has the least excess energy (Fig. 4), indicating that the relaxation competes with, or is masked by, state-filling from higher-lying levels. Additionally, the bleach intensity for higher-energy excitation never achieves the peak signal level we observe for the lowest-energy excitation.

We attribute this fast relaxation component to thermalization of the exciton over many fine structure states. As noted above, real world QD's exhibit fine structure within the electronic spectrum. Some of the near-band edge exciton states are spin-allowed, and others are not. Calculations reveal that, for 42 Å diameter InP QD's, the band edge fine structure consists of levels typically within 5 meV of one another.[17] Therefore, following absorption into spin-allowed states, the distribution of excitons within the sample will broaden to populate the many thermally accessible states, some of which exhibit considerably less oscillator strength. The result

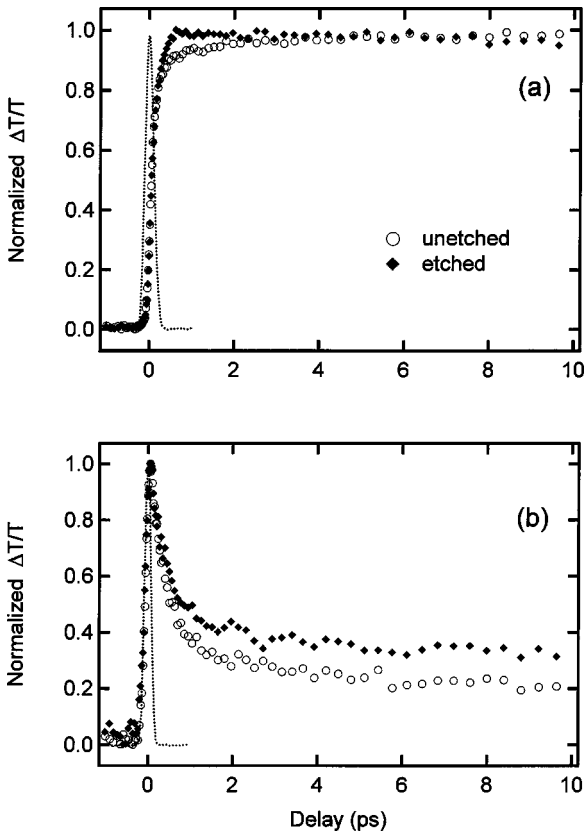

FIG. 5. Comparison of transient photoinduced bleaching of the (a) **S** and (b) **P** exciton peaks, at 1.88 and 2.15 eV, respectively, for etched and unetched InP QD samples. Photoexcitation at 2.30 eV and above excites the **P** exciton states. Relaxation to the *s*-like exciton states proceeds more quickly in the etched dots owing to better surface passivation by fluorine. Dotted curves show the cross-correlation in ZnO between pump and probe pulses.

is an aggregate depopulation of the absorbing transitions and thus a decrease in the **S** absorption bleach. Increasing the photoexcitation energy introduces exciton relaxation, a state-filling process which masks the effect of dispersion into spin-forbidden states. That the maximum **S** bleach is highest for low energy excitation suggests that relaxation from higher exciton states proceeds directly into spin-forbidden as well as spin-allowed states.

The landscape of InP QD trap states, both internal and surface-related, is quite complex.[20] Among the prominently identified trap states are surface and core electron traps (both due to phosphor vacancy), an additional deep electron trap at the surface due to oxygen, and a surface hole trap consisting of an indium vacancy.[12,20] While etching with HF is believed to passivate both types of surface electron traps, the surface hole trap is found to persist after etching. We attempt to study the effects of surface preparation on relaxation dynamics by comparing the **S** and **P** bleaching dynamics of our etched and unetched samples for photoexcitation at 2.30 eV (see Fig. 5). The unetched QD's are passivated with TOP/TOPO and, as indicated by the low band edge PL efficiency (Fig. 2), are affected by surface electron traps which appear largely passivated by the HF etch. As shown in Fig. 5(a), while the etched and unetched samples show **S** bleach signals which rise similarly for the first ~200 fs, the etched sample proceeds to complete its rise faster than does the unetched sample. The effect of etching on the bleach dynamics is small but reproducible. We are unable to determine here the origin of this effect, but the difference in rise time concurs with a model in which superior core confinement of the charge carriers, through surface state passivation, facilitates cooling via exciton-phonon interaction. Figure 5(b) shows the **P** peak bleach dynamics, measured at 578 nm (2.15 eV). Apart from the etched sample showing a larger bleach following the initial decay (e.g., after 5 ps), the dynamics of the **P** exciton bleach decay are very similar. We attribute the relatively poor correlation between the dynamics of the rise of the **S** bleach and decay of the **P** bleach to the complexity of the exciton electronic structure; contributions from the carrier-induced Stark effect further complicate analysis of the correlation.

Resolution of distinct exciton transitions near the first exciton transition has been challenging for colloidal InP QD's, owing to both the relatively large size distribution achieved by covalent chemistry synthesis of III-V QD's as well as the relatively small spin-orbit splitting in bulk InP which produces a higher state density near the valence band edge. Banin *et al.* applied transient nanosecond hole burning to 34 Å diameter InP QD's, and resolved the first exciton transition and also a second excited transition spaced at 100 meV, with a width of 100 meV.[21] Bertram *et al.* used PLE to map exciton transitions in InP QD's, characterizing the size dependence of eight distinct transitions.[22] Both of these characterizations were carried out at low temperatures ($\leqslant$20 K). Previous room temperature TA measurements of InP have revealed only a single, broad bleach peak associated with the lowest exciton transition.[10,17] Size-selective spectroscopy, based on reducing the photoexcitation photon energy to selectively excite only the largest dots within the distribution, has been used previously to narrow the size distribution of the sample that is photoexcited.[15,22] We have investigated the size-selective TA spectrum for our sample of etched InP QD's. Decreasing the excitation photon energy below that of the **S** bleach peak, we observe a redshifting of the spectrum as well as a slight narrowing of the spectral features. As we continue to tune the excitation to longer wavelengths beyond ~690 nm and to increase the intensity to compensate for decreasing sample absorption, the TA spectral features begin to once again broaden and show less size selection; this effect can be explained by increasingly significant two photon absorption which leads to an excitation at effectively twice the incident photon energy. The global TA spectrum, for photoexcitation at 370 nm, peaks at ~660 nm. In contrast, as shown in Fig. 6, size-selective excitation at 690 nm yields a TA spectrum (0.3 ps delay) which peaks at ~680 nm. The amplitude-normalized TA spectrum does not change markedly between delays of 0.3 and 20 ps (not shown), because the low excitation photon energy yields essentially no excited excitons. The 0.3 ps spectrum shown in Fig. 6 reveals a substantially asymmetric **S** bleach, indicating that two distinct transitions comprise the broader peak (which for increasing excitation photon energy merge into one more nearly symmetric peak). Open circles show the TA data, and

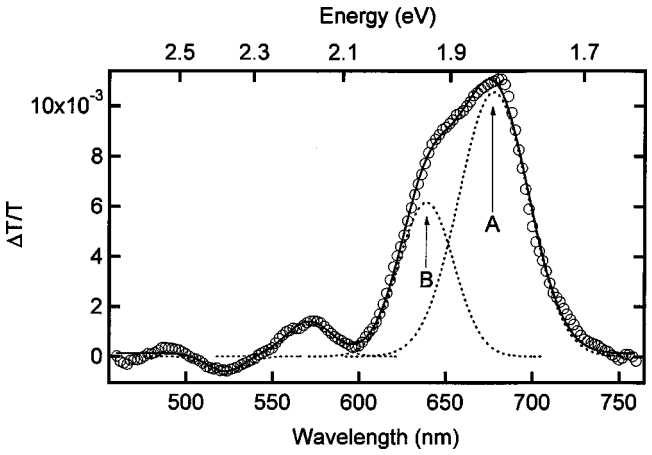

FIG. 6. The open circles show the transient absorption spectrum for the etched 42 Å diameter InP QD sample at 300 fs delay following size-selective 690 nm excitation. Asymmetry in the **S** exciton peak indicates the presence of two transitions. The dotted lines show the Gaussian fit components which when summed produce the solid line. Variations in the fit for multiple size-selected spectra yield an energy spacing between peaks **A** and **B** of 100 to 110 meV.

the solid line shows a fit to the data consisting of individual Gaussian components graphed as dotted lines. The resultant fit curves in Fig. 6 labeled **A** and **B** indicate the transitions we correlate to the two *s*-like exciton transitions. For this spectrum, transitions **A** and **B** show widths of 110 ± 5 meV and 70 ± 5 meV, respectively, and are spaced by 110 ± 5 meV. While the relative amplitudes of these peaks vary somewhat with sample and precise excitation wavelength, the spacing between them falls consistently within the range of ~105 to 115 meV, suggesting that with improving sample size distribution these two *s*-like exciton transitions will become increasingly distinct. While the observation of two *s*-like exciton transitions correlates very well with the calculated results, we do not observe evidence of a two-component **P** bleach peak; the calculated spacing between the *p*-like exciton peaks of 60 meV is slightly too small to resolve within our TA spectral data.

The width of the globally excited **S** bleach peak, shown as the solid line in Fig. 1, has three contributions (i) size inhomogeneity, (ii) underlying transition width, and (iii) broadening via dephasing through electronic coupling to QD core, surface, and solvent vibrational modes. While size inhomogeneity dominates the global TA spectrum, the size-selected TA spectrum shown in Fig. 6 does display two distinct peaks within the **S** bleach; as noted above, the widths of these transitions have been estimated using Gaussian peak fitting (Fig. 6). While the intrinsic linewidth has been predicted to be less than 0.1 meV even at room temperature, Banin *et al.* applied both nanosecond hole-burning (at 6 K) and three-pulse photon echo (at 20 K) to measure the effects of dephasing on the linewidth for InP QD's in the range of 29 to 34 Å diameter.[21] They found that dephasing through coupling to acoustic phonon modes limits the linewidth for these dot sizes to ~5 to 10 meV at 20 K. Although room temperature measurements have not been reported, the additional coupling to thermally active LO phonon modes is expected to broaden the transition energy widths significantly. Therefore, widths of several tens of meV may result from dephasing mechanisms.

CONCLUSIONS

Results of theoretical electronic structure calculations on 41.8 Å diameter InP quantum dots based on the atomistic pseudopotential method have been presented. By first calculating 32 conduction levels and 16 valence levels and including these in a configuration interaction calculation, seven major exciton transitions have been revealed. We identify the single particle states, including their envelope character, which contribute to the exciton transitions. Calculated exciton transitions are compared with the experimentally determined femtosecond TA spectrum, and excellent agreement is found. Femtosecond TA spectroscopy has been utilized to investigate the dynamics and spectral dependence of excitonic relaxation in colloidal InP quantum dots with average diameter of 42 Å. Following photoexcitation ~430 meV above the **S** bleach peak, electronic relaxation as evidenced by the rise time of the **S** bleach proceeds more efficiently for etched QD's, likely due to superior passivation of surface trap states. Varying the photoexcitation wavelength to increase the initial exciton energy above the *p*-like exciton energies results in slowed relaxation to the *s*-like exciton states. We also observe a fast initial relaxation process for excitation close to the first absorbing exciton state, and attribute the effect to thermalization of excitons into ''dark'' exciton levels which do not contribute to the absorption cross section. Finally, by tuning the photoexcitation energy to size-selectively pump larger dots in the sample, the broad **S** exciton peak exhibits asymmetry and structure indicative of two *s*-like exciton states, as expected from our theoretical calculations.

ACKNOWLEDGMENTS

The authors thank Olga I. Mićić for providing further insight into the nature of colloidal InP QD trap states. The authors from the National Renewable Energy Laboratory wish to thank the U.S. Department of Energy, Office of Science, Office of Basic Energy Sciences, Division of Chemical Sciences for generous financial support. H. Fu thanks the NSF for financial support (Grant No. DMR-0116315).

[1] H.-J. Eisler, V. C. Sundar, M. G. Bawendi, M. Walsh, H. I. Smith, and V. Klimov, Appl. Phys. Lett. **80**, 4614 (2002).

[2] A. Franceschetti, H. Fu, L. W. Wang, and A. Zunger, Phys. Rev. B **60**, 1819 (1999).

[3] We do not include here effects such as the electron-hole exchange interaction and crystal field splitting, both of which separate excitonic states to introduce ''fine structure.'' We therefore refer to exciton states which are derived from degenerate single-

particle levels.
[4] A. J. Nozik, Annu. Rev. Phys. Chem. **52**, 193 (2001).
[5] U. Bockelmann and G. Bastard, Phys. Rev. B **42**, 8947 (1990).
[6] H. Benisty, C. M. Sotomayor-Torres, and C. Weisbuch, Phys. Rev. B **44**, 10 945 (1991).
[7] P. Guyot-Sionnest, M. Shim, C. Matranga, and M. Hines, Phys. Rev. B **60**, R2181 (1999).
[8] V. I. Klimov, A. A. Mikhailovsky, D. W. McBranch, C. A. Leatherdale, and M. G. Bawendi, Phys. Rev. B **61**, R13 349 (2000).
[9] S. Xu, A. A. Mikhailovsky, J. A. Hollingsworth, and V. I. Klimov, Phys. Rev. B **65**, 045319 (2002).
[10] J. L. Blackburn, R. J. Ellingson, O. I. Micic, and A. J. Nozik, J. Phys. Chem. B **107**, 102 (2003).
[11] H. Fu and A. Zunger, Phys. Rev. B **55**, 1642 (1997).
[12] H. Fu and A. Zunger, Phys. Rev. B **56**, 1496 (1997).
[13] O. I. Micic, J. R. Sprague, Z. Lu, and A. J. Nozik, Appl. Phys. Lett. **68**, 3150 (1996).
[14] E. Poles, D. C. Selmarten, O. I. Micic, and A. J. Nozik, Appl. Phys. Lett. **75**, 971 (1999).
[15] O. I. Micic, H. M. Cheong, H. Fu, A. Zunger, J. R. Sprague, A. Mascarenhas, and A. J. Nozik, J. Phys. Chem. B **101**, 4904 (1997).
[16] O. I. Micic, S. P. Ahrenkiel, and A. J. Nozik, Appl. Phys. Lett. **78**, 4022 (2001).
[17] R. J. Ellingson, J. L. Blackburn, P. Yu, G. Rumbles, O. I. Micic, and A. J. Nozik, J. Phys. Chem. B **106**, 7758 (2002).
[18] V. I. Klimov and W. McBranch, Opt. Lett. **23**, 277 (1998).
[19] V. I. Klimov, A. A. Mikhailovsky, D. W. McBranch, C. A. Leatherdale, and M. G. Bawendi, Science **287**, 1011 (2000).
[20] O. I. Micic, A. J. Nozik, E. Lifshitz, T. Rajh, O. G. Poluektov, and M. C. Thurnauer, J. Phys. Chem. B **106**, 4390 (2002).
[21] U. Banin, G. Cerello, A. A. Guzelian, C. J. Bardeen, A. P. Alivisatos, and C. V. Shank, Phys. Rev. B **55**, 7059 (1997).
[22] D. Bertram, O. I. Micic, and A. J. Nozik, Phys. Rev. B **57**, R4265 (1998).